Fracture strength of ultrananocrystalline diamond thin films—identification of Weibull parameters

H. D. Espinosa,[a] B. Peng, B. C. Prorok, and N. Moldovan
Department of Mechanical Engineering, Northwestern University, Evanston, Illinois 60208-3111

O. Auciello, J. A. Carlisle, D. M. Gruen, and D. C. Mancini
Materials Science and Experimental Facilities Divisions, Argonne National Laboratory, Argonne, Illinois 60439

(Received 6 May 2003; accepted 5 August 2003)

The fracture strength of ultrananocrystalline diamond (UNCD) has been investigated using tensile testing of freestanding submicron films. Specifically, the fracture strength of UNCD membranes, grown by microwave plasma chemical vapor deposition (MPCVD), was measured using the membrane deflection experiment developed by Espinosa and co-workers. The data show that fracture strength follows a Weibull distribution. Furthermore, we show that the Weibull parameters are highly dependent on the seeding process used in the growth of the films. When seeding was performed with microsized diamond particles, using mechanical polishing, the stress resulting in a probability of failure of 63% was found to be 1.74 GPa, and the Weibull modulus was 5.74. By contrast, when seeding was performed with nanosized diamond particles, using ultrasonic agitation, the stress resulting in a probability of failure of 63%, increased to 4.13 GPa, and the Weibull modulus was 10.76. The tests also provided the elastic modulus of UNCD, which was found to vary from 940 to 970 GPa for both micro- and nanoseeding. The investigation highlights the role of microfabrication defects on material properties and reliability, as a function of seeding technique, when identical MPCVD chemistry is employed. The parameters identified in this study are expected to aid the designer of microelectromechanical systems devices employing UNCD films. © *2003 American Institute of Physics.* [DOI: 10.1063/1.1613372]

I. INTRODUCTION

The applications for current microelectromechanical system (MEMS) devices are limited because they are made almost exclusively from silicon. Silicon's limited mechanical and tribologial properties make it less than ideal for micromotors, micropumps, and other micromachines with fast-moving parts. To overcome this limitation, scientists are working to make these devices out of diamond, the hardest, most wear-resistant substance known. We have recently demonstrated that an ultrananocrystalline diamond (UNCD) coating technology developed at Argonne National Laboratory provides the basis for MEMS technology capable of yielding devices with superior performance.[1–4] UNCD has extremely small grain size (3–5 nm), significantly smaller than nanocrystalline diamond films (30–100 nm grain size) produced by the conventional CH_4/H_2 plasma chemistry.[2,3] The UNCD films posses many of the outstanding physical properties of diamond, i.e., they exhibit exceptional hardness, extremely low friction coefficient and wear, and high room temperature electrical conductivity when doped with nitrogen.[4] Preliminary results have shown that the microstructure of UNCD results in higher fracture strength compared with other materials like Si, poly-Si, SiC, microcrystalline diamond, and diamond like carbon[12,13] (see Table I). At present, the only material exhibiting better strength than UNCD is Si_3N_4.

Preliminary work by the authors has demonstrated the feasibility of fabricating two dimensional and three dimensional MEMS components that can be the basis for the fabrication of complete MEMS/ NEMS devices.[13–15] Components such as cantilevers and devices with multiple structural UNCD layers such as microturbines have already been produced.[16,17] These preliminary achievements are promising steps toward full-scale application of UNCD components in functional MEMS devices. However, before full-scale integration can occur, several intrinsic material properties, such as elastic modulus, plasticity, and fracture of undoped and doped UNCD must be well characterized to fully exploit the potential of this material. In this article, we use the membrane deflection techniques developed by Espinosa and co-workers[18] to gain a better understanding of the fracture strength of UNCD thin films.

Several microscale testing techniques have been employed to investigate fracture strength of thin films. Sharpe *et al.*[19,20] and Bagdahn and Sharpe[23] have performed microsample tension tests to study the fracture strength of SiC and polysilicon.[10,19,20] The specimens are manufactured by surface micromachining with one end attached to the silicon wafer. The gage section and the grip end of the specimen are released by etching away the underlying sacrificial layer. The nominal dimensions of the gage sections are 6 and 20 μm

[a]Author to whom correspondence should be addressed; electronic mail: espinosa@northwestern.edu

TABLE I. Fracture strengths of other hard materials.

Material	Fracture strength (GPa)
Silicon[a]	0.30
Diamond-like carbon[b]	0.70
Microcrystalline diamond[c]	0.88 ± 0.12
SiC[d]	1.2 ± 0.5
Polysilicon[e]	1.5 ± 0.25
Single Crystal Diamond[f]	2.8
UNCD [Previous and current work][g]	4.13 ± 0.90
Si_3N_4[h]	6.41 ± 1.04

[a]See Ref. 5.
[b]See Ref. 6.
[c]See Ref. 7.
[d]See Ref. 8.
[e]See Ref. 9, 10.
[f]See Ref. 11.
[g]See Ref. 12, 13.
[h]See Ref. 14.

wide, 250 and 1000 μm long, and 1.5, 2, and 3.5 μm thick. In the technique developed by Sharpe and co-workers, a probe is attached to the grip end of the specimen, which is pulled by a piezoelectric translation stage. Force is measured with a 100 g load cell and overall system displacement is measured with a capacitance probe. The strain is measured directly on the specimen via laser interferometry. Young's modulus is extracted from the force–displacement record by comparing the records of specimens of different lengths to eliminate the need to know the system stiffness. Using this technique, the strength of several thin film materials were determined. For polysilicon, the measured strength was found to be highly dependent on the film deposition parameters. A strength of 1.56 ± 0.25 GPa was measured for the Cronos process, 2.85 ± 0.40 GPa for the Sandia process, and 2.04 ± 0.30 GPa for the SMI process. The fracture strengths of SiC was measured to be 1.2 ± 0.5 GPa for the Case Western Reserve University process and 0.49 ± 0.2 GPa for the Massachusetts Institute of Technology process.

Chasiotis and Knauss[21,22] performed tensile tests, using a sample geometry and loading stage similar to the one used by Sharpe and co-workers, to investigate the mechanical strength of polysilicon films.[21,22] The ''dog-bone-shaped'' tensile microspecimens were designed with test section dimensions of length$=400\ \mu$m, width$=50\ \mu$m, and thickness$=2\ \mu$m, attached to a silicon substrate. The displacements are imposed to the specimen via an inchworm actuator that is powered by a personal computer and a dedicated controller. The controller provides a measurement of the system displacement with an accuracy of 4 nm for every single step of the actuator. The induced load is measured by a miniature tension/compression load cell with an accuracy of 10^{-4} N and maximum capacity of 0.5 N. The local deformation is monitored directly on the specimen surface by means of atomic force microscope (AFM) digital image correlation. These researchers measured a fracture strength of 1.3 ± 0.1 GPa for the Cronos process. This value is slightly smaller than the one measured by Sharpe *et al.*

The lack of ductility or yielding of SiC and polysilicon leads to three characteristic features: (1) large data scatter, (2) small strain to failure, and (3) relatively low fracture strength. To interpret the scatter in the data of fracture strength, both Sharpe[23] and Knauss[24] used a probabilistic theory known as the ''weakest link,'' which was first introduced by Weibull.[25]

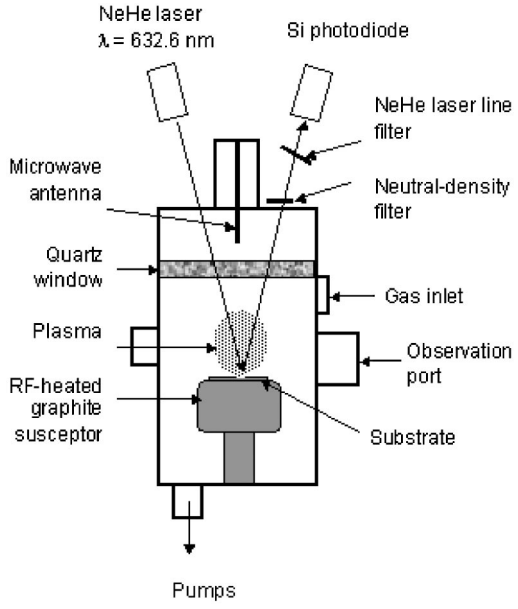

FIG. 1. Schematic diagram of the 2.45 GHz microwave chamber showing a plasma ball in contact with a substrate and heated stage. The total pressure is 100 Torr, and the microwave power is 600–800 W.

Due to the fact that UNCD will be used to fabricate ultrasmall structures (micro/nanoscale) and the UNCD grain size is 3–5 nm, it is necessary to characterize its properties using microscale compatible techniques to probe the properties of this material at the appropriate scale. For this purpose, the membrane deflection experiment (MDE) is here used in the investigation of strength of submicron freestanding UNCD thin films. In this article we describe the UNCD film processing, microfabrication steps used in the preparation of MDE specimens, the testing methodology, and the identified Weibull parameters.

II. THE MATERIALS

The UNCD films are grown by a microwave plasma enhanced chemical vapor deposition synthesis method developed at Argonne National Laboratory that involves argon rich CH_4/Ar plasma chemistries,[2] where C_2 dimers are the growth species derived from collision induced fragmentation of CH_4 molecules in an Ar plasma. The UNCD film growth proceeds via the reactions $2CH_4 \rightarrow C_2H_2 + 3H_2$; $C_2H_2 \rightarrow C_2 + H_2$, in atmospheres containing very small quantities of hydrogen.

A gas mixture of Ar (99%) and CH_4 (1%) is fed into a microwave cavity (ASTeXPDS-17) as shown in Fig. 1. Mixtures of CH_4, Ar, and H_2 are used as the reactant gases for the microwave discharges. During the deposition process, the substrate temperature, which was controlled by a separate heater, was maintained at 800 °C, while total ambient pressure and input power were kept at 100 Torr and 1200 W, respectively.

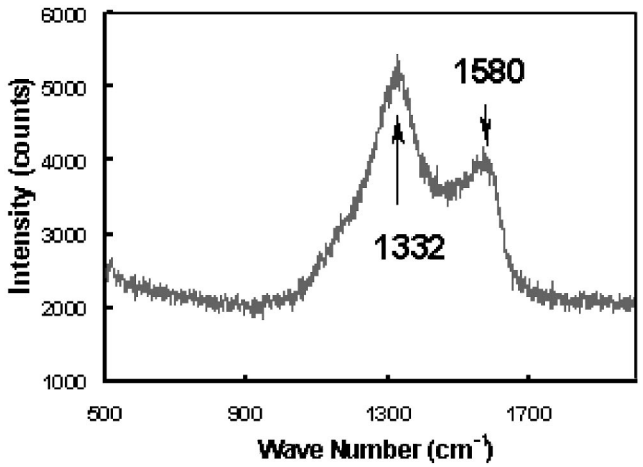

FIG. 2. A Raman spectrum taken from an UNCD-coated Si surface reveals a sharp intense feature at 1332 cm^{-1} overlapped with a broad peak associated with the UNCD. The feature at 1580 cm^{-1} corresponds to sp^2 bonded carbon.

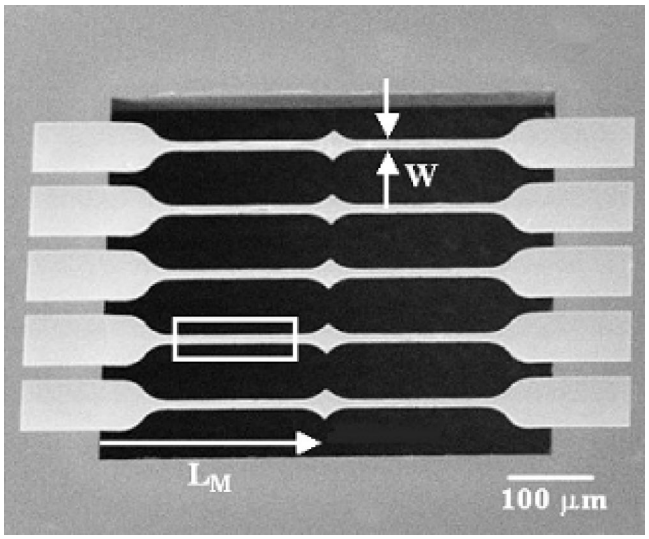

FIG. 4. SEM image of five UNCD membranes showing characteristic dimensions. L_M is half the membrane span, and W is the membrane width. The gage region is highlighted by a rectangular box.

Under these conditions, diamond films grow on substrates seeded with diamond particles on a heated stage in contact with the plasma. Raman analysis is conducted to examine the film chemistry. Figure 2 shows a Raman spectrum taken from the center region of the sample, as is typical of UNCD films grown at 800 °C. All the spectral features shown in Fig. 2 arise from carbon that is not sp^3 bonded, but derived from atoms located within the grain boundaries which are 0.2–0.5 nm wide. Detailed high-resolution transmission electron microscopy studies[26] and synchrotron measurements[27] have confirmed that UNCD consists of more than 95% sp^3 bonded carbon.

To enhance the nucleation of vapor species the diamond powders are seeded using two techniques:

(1) microseeding: microsize diamond particles are seeded on the silicon substrate by means of mechanical polishing and
(2) nanoseeding: nanosize particles are seeded on the silicon substrate using ultrasonic agitation in a bath containing nanodiamond powder.

III. MICROFABRICATION OF FREESTANDING UNCD SPECIMENS

The specimen geometry utilized in this study resembles the typical dog-bone tensile specimen but with an area of additional width in the center designed as the contact area where the line load is applied, Fig. 3.[18] This feature is used to minimize stress concentrations where the loading device contacts the membrane.

The suspended membranes are fixed to the wafer at either end such that they span the bottom view window (Fig. 4). In the areas where the membrane is attached to the wafer and in the central contacting area the width is varied in such a fashion to minimize boundary-bending effects. These effects are also minimized through large specimen gauge lengths. Thus, a load applied in the center of the span results in direct stretching of the membrane in the areas of thin constant width in the same manner as in a direct tension test. In this study membranes with dimension of $L_M = 350\ \mu m$ and $W = 18\ \mu m$ were tested. The thickness of the membranes

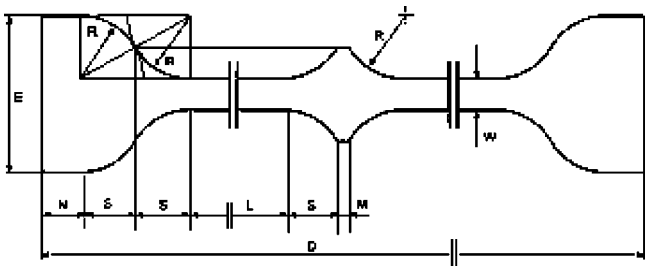

FIG. 3. Schematic of membrane geometry indicating the different parameters used to define specimen dimensions, where $E = 100\ \mu m$, $R = 40\ \mu m$, $W = 20\ \mu m$, $N = 100\ \mu m$, $L = 200\ \mu m$, $S = 34.64\ \mu m$, $M = 10\ \mu m$, and $D = 817.84\ \mu m$.

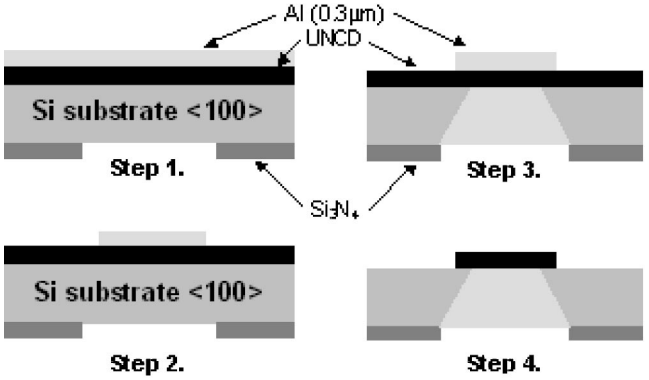

FIG. 5. Cross-sectional view of the microfabrication steps to obtain freestanding UNCD membranes.

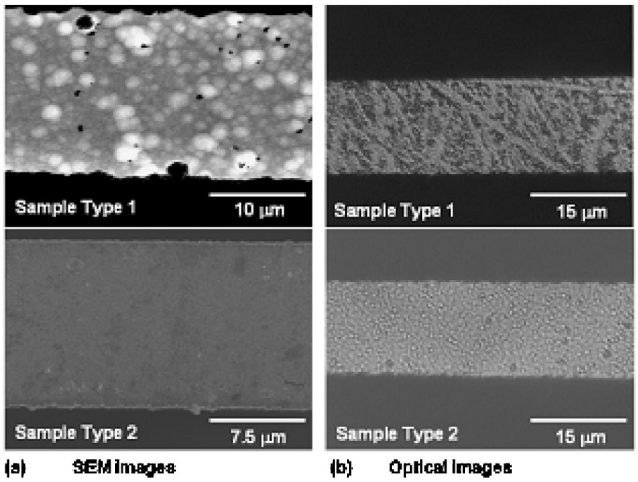

FIG. 6. (a) SEM images of samples type 1 and type 2. Sample type 1 has many holes scattered all around the film; by contrast sample type 2 has no holes. In addition, the edges of sample type 1 exhibit significant waviness. (b) Optical images of both samples showing that mechanical seeding results in many scratches-like surface features. No such features are observed in the nanoseeding UNCD film.

varied from 600 to 800 nm. The MDE specimens were microfabricated using standard procedures. The following is a summary of the steps (Fig. 5).

(1) Growth of UNCD on silicon substrate (~1.0 μm). Deposition of 300 nm Al by sputtering. Al is used as mask material due to its resistance to oxygen reactive ion etching (RIE). Deposition and patterning of Si_3N_4 (~0.5 μm) on the bottom side of the silicon wafer used as a mask for KOH etching of silicon.
(2) Photoresist spin coating with S1805 and prebaking, exposure with mask aligner (Karl Suss MA6), resist development and postbaking, and wet chemical etching of Al.
(3) KOH etching from backside, 9 h (KOH 30% at 80 °C). The UNCD film is used as etching stop layer to define windows under the membranes.
(4) O_2 RIE, 50 mTorr, 200 W, various times, until the exposed UNCD is etched away. During the etching, the photoresist is also removed. Removal of the Al mask is accomplished by wet etching.

Two sample types are prepared to compare the fracture strength of specimens grown by the two seeding techniques with sample type 1 using mechanical seeding (microseeding) and sample type 2 using solution ultrasonic seeding (nanoseeding). Top surface scanning electron microscopy (SEM) images of the specimen gage region revealed that sample type 1 has poor nucleation and results in film porosity [Fig. 6(a)].

In fact, the mechanical seeding leaves scratches on the surface of the UNCD film [Fig. 6(b)] greatly reducing the mechanical strength of the membranes as will be shown later. In addition, a roughness analysis was conducted on supported areas of the membrane using AFM (Fig. 7). Sample type 1 has a mean square root (rms) roughness of 107 nm and a distance from peak to valley of 250–300 nm. Sample type 2 has a rms of 20 nm and a distance from peak to valley of ~70 nm. Clearly, nanoseeding results in much better nucleation and growth, no obvious porosity, no scratches, and enhanced surface smoothness. These characteristics significantly improve the mechanical strength of UNCD as will be shown in Sec. V.

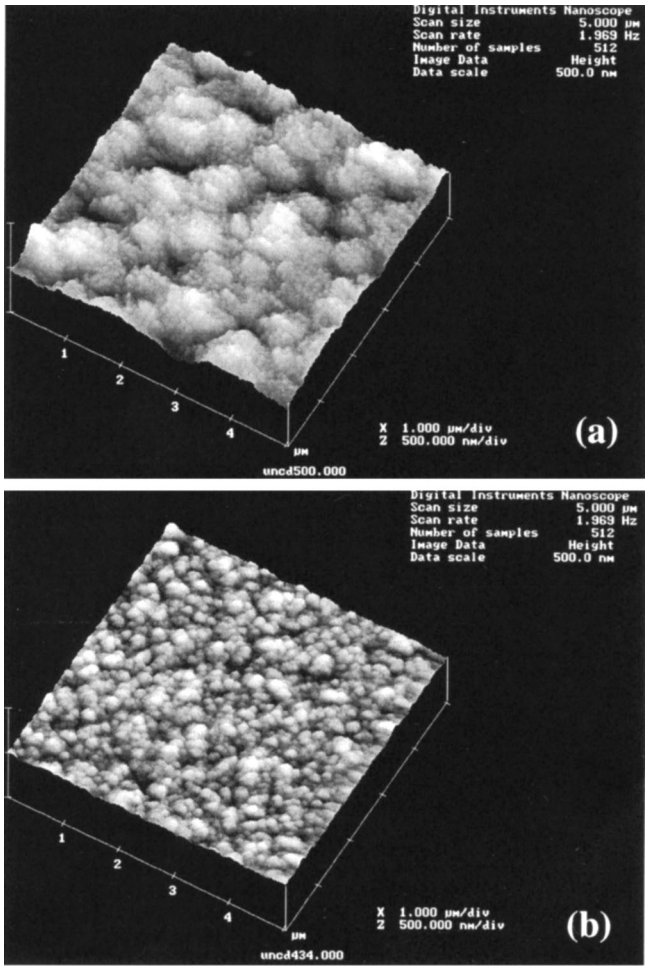

FIG. 7. Roughness analysis of UNCD surfaces using AFM. (a) Sample type 1 has a mean square root (rms) roughness of 107 nm and a distance from peak to valley of 250–300 nm. (b) Sample type 2 has a rms of 20 nm with a distance from peak to valley of ~70 nm.

IV. EXPERIMENTAL METHODOLOGY

The MDE was used to achieve direct tensile stressing of the specimens. In this procedure, a line load is applied with a nanoindenter to the center of the spanning membrane. Simultaneously, an interferometer focused on the bottom side of the membrane records the deflection. The result is direct tension in the gauge regions of the membrane with load and deflection measured independently. A schematic of the membrane deflection experimental setup is shown in Figs. 8(a) and 8(b). It consists of a nanoindenter, to apply load to the center of the membrane from the top, and a Mirau microscope interferometer positioned directly below the specimen to independently measure deflection through the microfabricated die window. A combined nanoindenter and AFM apparatus was used in this investigation to characterize the specimen geometry and load the membranes. The typical experimental procedure can be described in three steps. The

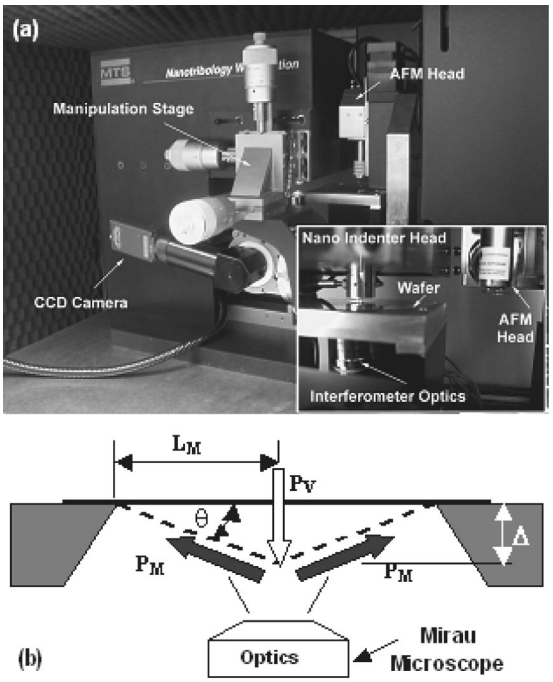

FIG. 8. (a) The topside view of the combined Nanoindenter/AFM experimental setup. (b) Side view of the MDE test showing vertical load being applied by the nanoindenter, P_V, the membrane in-plane load, P_M, and the position of the Mirau microscope objective.

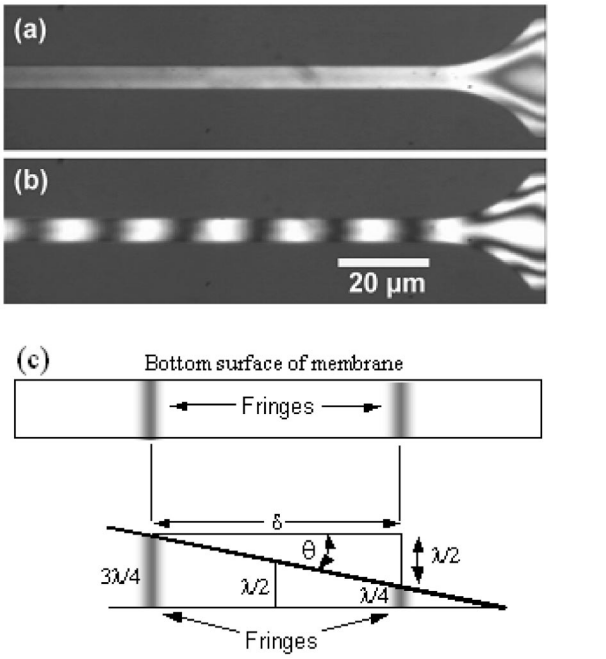

FIG. 9. Monochromatic images of the bottom side of the membranes showing an unloaded membrane (a) and a membrane under load which has developed fringes (b). (c) is a schematic representation showing the relationship between distance between fringes (δ) and vertical displacement. The distance between fringes is taken at the central points of the dark bands (see Ref. 18).

first step is to locate and characterize the membrane geometry by means of the optical and scanning capabilities of the AFM.

Once the profile and surface geometry are stored, the wafer is moved to the test position to begin the second step. This is accomplished by means of an $x-y$ translation stage with a positioning accuracy of 1 μm or better. The second step is the MDE itself. Parameters are set and a drift test is executed. Once the test criterion is reached, the membrane is loaded. Simultaneously, the aligned interferometric station is focused on the back surface of the film. The camera is then set to acquire digital images within a desired period of time. Force and displacement data are stored in the Nanoindenter controller PC, and full field displacements are stored by acquiring monochromatic images. Prior to acquiring each set of images, the focus on the surface is updated to correct for the out-of-plane motion resulting from the downward displacement of the membrane.

The third step of the experiment is data reduction. Using the measured distance between fringes, obtained from the interferometer, and load and deflection data, obtained from the nanoindenter measurements, nominal stress and strain are independently computed.

The data directly obtained from the MDE test must then be reduced to arrive at a stress–strain signature for the membrane. The load in the plane of the membrane is found as a component of the vertical nanoindenter load by the following equation:

$$\tan\theta = \frac{\Delta}{L_M}$$

and

$$P_M = \frac{P_V}{2\sin\theta}, \tag{1}$$

where [from Fig. 8(b)] θ is the angle of deflection, Δ is the displacement, L_M is the membrane half length, P_M is the load in the plane of the membrane, and P_V is the load measured by the nanoindenter. Once P_M is obtained the nominal stress $\sigma(t)$ can be computed from

$$\sigma(t) = \frac{P_M}{A}, \tag{2}$$

where A is the cross-sectional area of the membrane in the gauge region. The cross-sectional area dimensions are measured using AFM.

As the membrane is deflected by the nanoindenter, the interferometer, which works based on the Michelson interferometer principle, records the membrane deflection by resolving surface fringes. A fringe will occur at each λ/2 change in vertical height of the membrane. The relationship between the distance between fringes, δ, and vertical displacement is shown in Fig. 9.

Assuming that the membrane is deforming uniformly along its gauge length, the relative deflection between two points can be calculated, independently of the nanoindenter measurements, by counting the total number of fringes and multiplying by λ/2. Normally, part of the membrane is out of the focal plane and thus all fringes cannot be counted. We find the average distance between a number of fringes that are in the focal plane and then compute the angle θ_1. The average fringe distance, within the specimen gage region, is

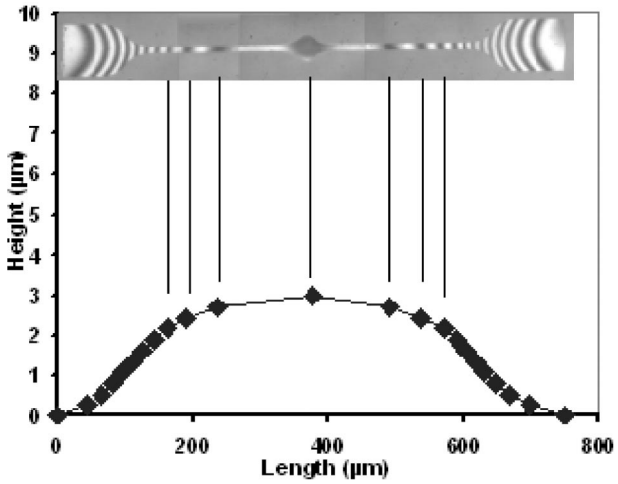

FIG. 10. Interferometric characterization showing the out-of-plane bulging of the freestanding UNCD membranes.

then obtained as $\delta = 0.5\lambda/\tan\theta_1$. From this information an overall strain, $\varepsilon(t)$, for the membrane can be computed from the following relation, viz.:

$$\varepsilon(t) = \frac{\sqrt{\delta^2 + (\lambda/2)^2}}{\delta} - 1. \tag{3}$$

An important aspect of the UNCD MDE specimens was that each membrane bowed upward as processed, i.e., out of the wafer plane. This is believed to result from the difference in thermal expansion coefficients, between the film and Si wafer, such that cooling down from the deposition temperature, approximately 800 °C, resulted in the Si shrinking more than the UNCD film. The film curvature is indicative of a gradient of residual stresses across the film thickness. Figure 10 shows a typical interferometric image and the as generated $x-z$ profile. This profile was obtained from the knowledge that the vertical distance between two dark fringes is half of the wavelength of the monochromatic green light used in the imaging ($\lambda/2 = 270$ nm). From this profile the height above the plane of the wafer, Δ_c, was determined. Also, the profile was used to measure the actual length of the curved membrane, which is used to determine the downward deflection, Δ_s, corresponding to the beginning of uniform specimen straining (see Fig. 11).

V. RESULTS AND DISCUSSION

The stress–strain behavior obtained in a typical test is shown in Fig. 12(a). As mentioned above, the curve begins at a deflection where the membrane becomes stressed in pure tension, point 3 in Fig. 11(b). The slope of the plot represents the elastic modulus, which was found to be 950 GPa. Modulus varied from 940 to 970 GPa for both sample type 1 and sample type 2. Failure stress varied in a statistical manner. The fracture stress of type 1 specimens was in the range of 0.89–2.42 GPa. These values are low considering that UNCD possesses a very high elastic modulus. We attribute this low fracture value to the defects (see Fig. 3) that originate from the seeding process employed to grow the UNCD

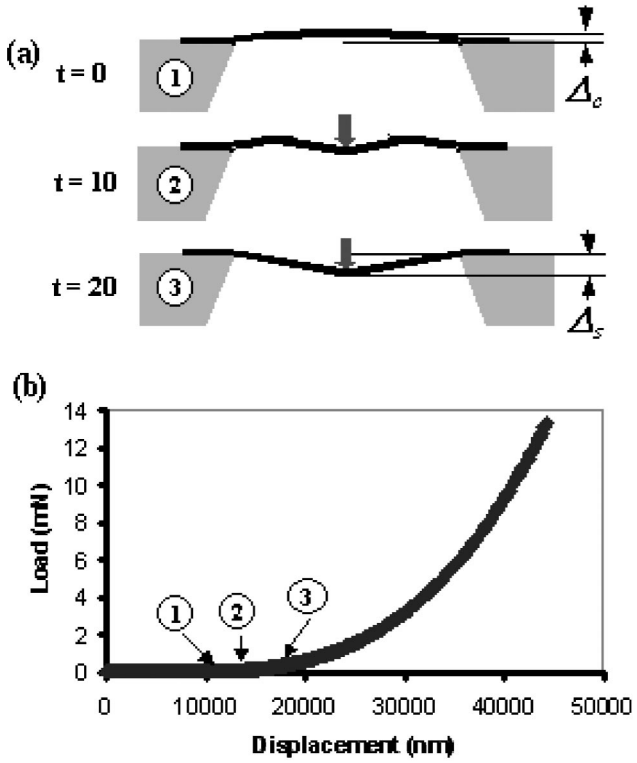

FIG. 11. (a) Schematic representations of the side view of the MDE test at three different time intervals. Δ_c is the vertical displacement at the middle of the span and Δ_s is the deflection at which uniform straining of the membrane begins. (b) Representation of the three states shown in (a) on the load–displacement curve.

films. Sample type 2 has improved fracture strength with failure stress values in the range 2.92–5.03 GPa.

In all specimens tested by MDE, failure occurred in the gauged region. This is illustrated in Fig. 12(b). In this SEM image, five tested membranes are shown. All the membranes failed in both gauge regions except for the second one that failed on the upper gauge leaving the specimen intact. These images provide confidence that the controlling factors in the membrane behavior were confined to the gauged region. As the variation in strength comes from a variation in the size of the biggest defect, it is believed that the failure occurs at the biggest defect within the specimen.

This is the reason why fracture occurs randomly in the gauge region. Figure 13 shows an enlarged SEM image of the fracture surface of one of the tested membrane shown in Fig. 12(b). Three regions of the fracture surface were examined at a higher magnification. Zoom 1 shows a relatively smooth surface with no defects that can be associated to crack initiation. Zoom 2 shows a large defect, which could be a possible fracture origin, and a rougher surface. Zoom 3 shows additional features of the crack surface such as river-like features.

UNCD is a brittle material displaying a linear stress–strain response from zero strain to fracture as we can see from Fig. 12(a). Lack of ductility or yielding leads to large data scatter in strength. The fracture strength of UNCD is determined by a combination of material microstructure and a variable defect size. As the fracture toughness is not vari-

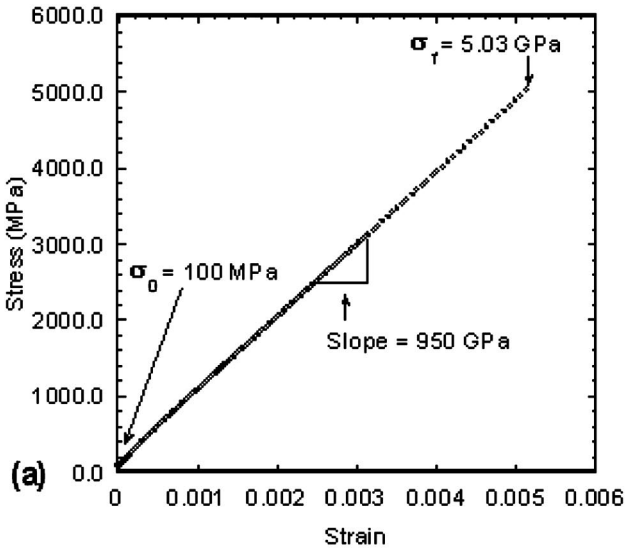

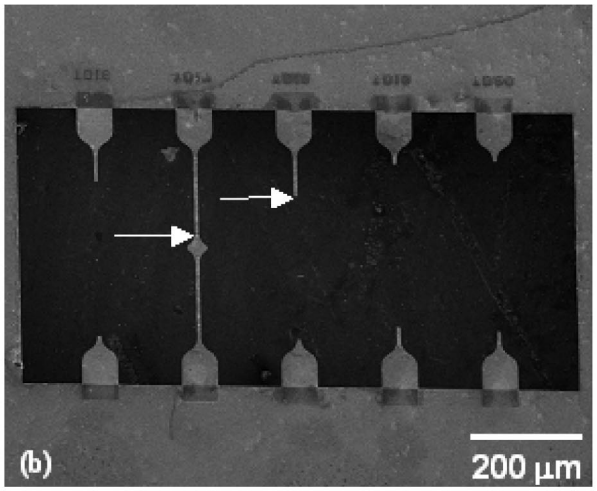

FIG. 12. (a) Stress–strain curve representative of the behavior exhibited by a typical UNCD MDE sample. (b) SEM image of five MDE specimens after testing. The image illustrates that failure indeed occurs in the gauge regions and mostly at two locations.

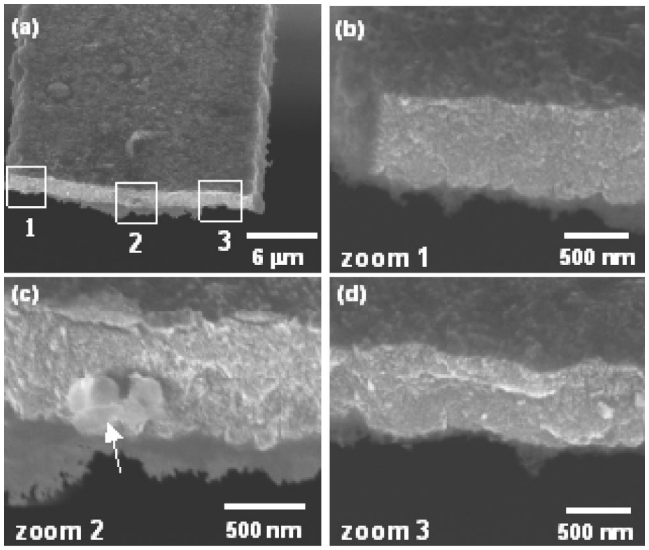

FIG. 13. SEM image of the fracture surface of a tested UNCD membrane (a). (b), (c), and (d) show three magnified windows along the fracture surface (zoom 1, zoom 2, and zoom 3, respectively). There is a big defect in zoom 2 that could be the fracture origin. The defect is faceted consistent with a large diamond crystal.

able, the variation must come from a variation in the size of the biggest defect. This is the reason why it is not possible to define the strength of UNCD as a constant material property but rather in terms of statistical parameters.

It is known that the strength distribution of brittle materials does not follow a Gaussian distribution. Failure is described by the widely used Weibull cumulative function.[28–30] Weibull statistics allows examination of strength values in the sense of failure probability at a certain stress level. The Weibull distribution is defined as

$$P_f(V) = 1 - \exp\left[-\frac{V}{V_0}\left(\frac{\sigma - \sigma_u}{\sigma_0} \right)^m \right], \tag{4}$$

where σ is the failure stress, σ_0 is the stress scaling parameter, in other words, it is the stress that would result in 63%, $(1-e^{-1})\cdot 100\%$, of the specimens to fail, m is the Weibull modulus, which can be identified from a log–log plot of the probability of failure, σ_u is a threshold stress, and V_0 is the reference volume on which the Weibull parameters are identified. Here V/V_0 is assumed to be unity since the volume of the specimens was constant.

Weibull plots are often used in the design of products to estimate the cumulative probability at which a given component will fail under a given load. These plots are based on data obtained on a representative population of samples and, where possible, tested in a manner similar to that the products will experience during their lives. Thirty-four UNCD membranes for each sample type (micro- and nanoseeding) were tested under the same environment using the MDE technique, with a higher than 97% success rate of failure. The average Young's modulus for all experiments was 953 $\pm$15 GPa.

The failure probability at a given stress is found by[31]

(1) ranking the failure stresses in order of strength and
(2) assigning a probability of failure $P_f = n/(N+1)$ to the nth ranked specimen in a total sample size of N.

The fracture stresses and failure probability of sample type 1 and sample type 2 are listed in Table II.

The results of the failure strength measurements are shown in Fig. 14. From plots of probability of failure and strength, σ_u was found to be 0.66 and 2.2 GPa for micro- and nanoseeding samples, respectively. The scaling parameter σ_0 was identified as 1.74 GPa for sample type 1 and 4.18 GPa for sample type 2, respectively. Both sets of data fit the Weibull distribution fairly well. From the Weibull plot we can see that the strength of UNCD is heavily dependent on the quality of the seeding process, i.e., surface smoothness and seeding-induced defects.

From the plot of ln(strength) and $\ln[-\ln(1-P_f)]$ (Fig. 15), the Weibull modulus, m, can be determined as the slope of the curve. This parameter defines the shape of the failure distribution curve. When m is large, the distribution is nar-

TABLE II. Experimental fracture strength of tested specimens and calculated failure probability.

Rank order	Sample type 1 strength (GPa)	Sample type 2 strength (GPa)	Failure probability
1	0.89±0.12	2.92±0.07	0.029
2	1.16±0.15	3.47±0.08	0.057
3	1.20±0.16	3.52±0.08	0.086
4	1.21±0.16	3.53±0.08	0.114
5	1.28±0.17	3.59±0.08	0.143
6	1.33±0.17	3.60±0.08	0.171
7	1.34±0.17	3.62±0.08	0.2
8	1.34±0.18	3.63±0.08	0.229
9	1.40±0.18	3.63±0.08	0.257
10	1.41±0.18	3.64±0.08	0.285
11	1.44±0.19	3.72±0.09	0.314
12	1.45±0.19	3.92±0.09	0.343
13	1.45±0.19	3.94±0.09	0.371
14	1.47±0.19	3.94±0.09	0.4
15	1.56±0.20	3.95±0.09	0.429
16	1.59±0.21	3.97±0.09	0.457
17	1.60±0.21	3.98±0.09	0.486
18	1.61±0.21	4.00±0.09	0.514
19	1.66±0.21	4.08±0.09	0.543
20	1.70±0.22	4.16±0.09	0.571
21	1.70±0.22	4.17±0.09	0.6
22	1.70±0.22	4.17±0.09	0.629
23	1.73±0.22	4.18±0.09	0.657
24	1.77±0.23	4.18±0.09	0.686
25	1.79±0.23	4.19±0.09	0.714
26	1.81±0.23	4.19±0.09	0.743
27	1.84±0.24	4.22±0.10	0.771
28	1.84±0.24	4.24±0.10	0.8
29	1.96±0.25	4.27±0.10	0.829
30	1.98±0.25	4.29±0.10	0.857
31	2.00±0.26	4.29±0.10	0.886
32	2.02±0.26	4.30±0.10	0.914
33	2.03±0.26	4.51±0.10	0.943
34	2.26±0.29	5.03±0.11	0.971

row, showing a small spread of failure strength, reliable material. When m is small, the distribution is wide showing a large variation in failure strength, unreliable material. Poor ceramics have m in the range 3–5. Good engineering ceramics have m values in the range 10–40, usually closer to 10 except for high toughness materials. The data reported in

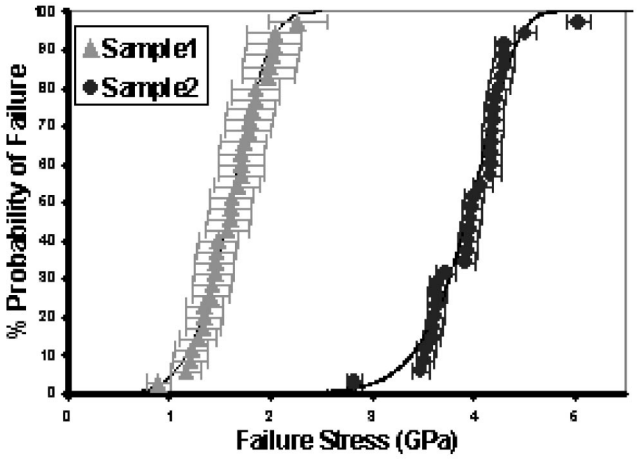

FIG. 14. Weibull plots for UNCD samples type 1 and 2.

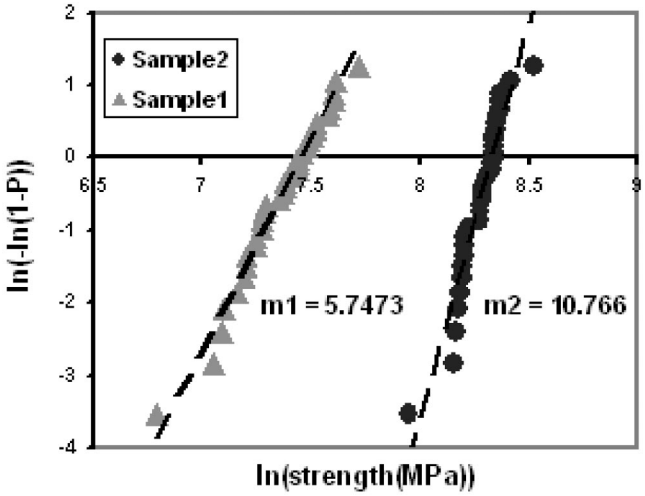

FIG. 15. Weibull exponent, m, for UNCD samples type 1 and 2.

Fig. 15 clearly show that specimens grown using microseeding exhibited poor reliability. By contrast, specimens grown using nanoseeding fall into the definition of reliable materials.

VI. CONCLUDING REMARKS

In this work, the membrane deflection experimental technique was employed to characterize the fracture strength of UNCD freestanding thin films. Two seeding types were employed. It was asserted that the fracture strength of UNCD could be analyzed with a Weibull statistic distribution as the variation in strength originates from a variation in the size of the biggest defect in a given volume of material. For microseeding UNCD, the fracture strength was found to be 1.74 and 2.26 GPa for failure probabilities of 63% and 97%, respectively. Using an improved seeding technique, ultrasonic coating of Si substrates with nanodiamond powder, the fracture strength was found to increase to 4.08 and 5.03 GPa for failure probabilities of 63% and 97%, respectively. Current work underway, including substantial improvement in the seeding and deposition processes, will provide UNDC films with much reduced defect sizes that will enable us to approach more closely the intrinsic fracture strength of the material. This work will be reported in a forthcoming article.

In this work, the strength of the material was assessed using a constant specimen volume. Future work will examine the strength of specimens with a range of volumes in order to fully examine the applicability of the Weibull theory of failure. At present, the limitations of the theory are not well understood and one would expect that by interrogating smaller and smaller volumes the defect distribution would be highly dependent on the material microstructure and its variability.

The measured fracture strength of UNCD using nanoseeding is much higher than that of polysilicon (1.56 GPa) and SiC (1.44 GPa). The fracture properties of UNCD films established in this work indicate that UNCD films can be advantageously used in MEMS devices.

The work here reported highlights the relevance of the seeding process in the growth of diamond films and its effect

on mechanical properties. Additional improvement could in principle be achieved, which are expected to further increase the average strength and reliability of the material.

ACKNOWLEDGMENTS

The authors would like to acknowledge the contributions of J. E. Gerbi, James Birrell, X. Xiao, and M. Angadi in the deposition of the UNCD films and the development of the nanoseeding technique. This work was sponsored by the National Science Foundation under Career Award No. CMS-9624364 and under GOALI Award No. CMS-0120866/001. Work was also supported in part by the Nanoscale Science and Engineering Initiative of the National Science Foundation under NSF Award No. EEC-0118025 and by DOE Office of Science under Contract No. N00014-97-1-0550.

[1] D. M. Gruen, Annu. Rev. Mater. Sci. **29**, 211 (1999).
[2] D. M. Gruen, S. Liu, A. R. Krauss, J. Luo, and X. Pan, Appl. Phys. Lett. **64**, 1502 (1994).
[3] D. M. Gruen, S. Liu, A. R. Krauss, and X. Pan J. Appl. Phys. **75**, 1758 (1994).
[4] B. Bhattacharyya *et al.*, Appl. Phys. Lett. **79**, 1441 (2001).
[5] K. E. Peterson, Proc. IEEE **70**, 5 (1982).
[6] S. Christiansen, M. Albrecht, and H. P. Strunk, J. Mater. Res. **11**, 8 (1996).
[7] G. F. Cardinale and C. J. Robinson, J. Mater. Res. **7**, 6 (1992).
[8] K. M. Jackson, R. L. Edwards, G. F. Dirras, and W. N. Sharpe, Mater. Res. Soc. Symp. Proc. **687**, 631 (2002).
[9] W. N. Sharpe, Jr., K. M. Jackson, K. J. Hemker, and Z. Xie, J. Microelectromech. Syst. **10**, 3 (2001).
[10] W. N. Sharpe, Jr., K. Jackson, G. Coles, and D. A. LaVan, Mater. Res. Soc. Symp. Proc. **657**, 51 (2001).
[11] J. E. Field, *The Properties of Diamond* (London, 1979).
[12] B. C. Prorok, H. D. Espinosa, B. Peng, N. Moldovan, D. M. Gruen, O. Auciello, J. A. Carlisle, and D. C. Mancini, J. Exp. Mech. (in press).
[13] H. D. Espinosa, B. C. Prorok, K.-H. Kim, B. Peng, O. Auciello, J. A. Carlisle, D. M. Gruen, N. Moldovan, and D. C. Mancini, Mater. Res. Soc. Symp. Proc. **741**, 42 (2002).
[14] G. Coles, W. N. Sharpe, Jr., and R. L. Edwards, Soc. Exp. Mech. **1–4**, 176 (2001).
[15] O. Auciello *et al.*, Mater. Res. Soc. Symp. Proc. **605**, 78 (2000).
[16] A. R. Krauss *et al.*, Diamond Relat. Mater. **10**, 1952 (2001).
[17] N. Moldovan *et al.*, Proc. SPIE **4557**, 288 (2001).
[18] H. D. Espinosa, B. C. Prorok, and M. Fischer, J. Mech. Phys. Solids **51**, 67 (2003).
[19] W. N. Sharpe, Jr., K. T. Turner, and R. L. Edwards, J. Exp. Mech. **39**, 3 (1999).
[20] W. N. Sharpe, Jr., K. M. Jackson, K. J. Hemker, and Zielang Xie, J. Microelectromech. Syst. **10**, 3 (2001).
[21] I. Chasiotis and W. G. Knauss, Proc. SPIE **4175**, 2 (2000).
[22] I. Chasiotis and W. G. Knauss, Mater. Res. Soc. Symp. Proc. **657**, 221 (2001).
[23] J. Bagdahn and W. N. Sharpe, Jr., Mater. Res. Soc. Symp. Proc. **687**, 971 (2002).
[24] D. A. LaVan, T. Tsuchiya, G. Coles, W. G. Knauss, I. Chasiotis, and D. Read, ASTM Spec. Tech. Publ. **1413**, 10 (2001).
[25] T. T. Shih, Eng. Fract. Mech. **13**, 257 (1980).
[26] J. Birrell, J. A. Carlisle, O. Auciello, D. M. Gruen, and J. M. Gibson, Appl. Phys. Lett. **81**, 2235 (2002).
[27] D. M. Gruen *et al.*, Appl. Phys. Lett. **68**, 1640 (1996).
[28] B. R. Lawn, *Fracture of Brittle Solids*, 2nd ed. (Cambridge University Press, Cambridge, 1993).
[29] J. D. Sullivan and P. H. Lauzon, J. Mater. Sci. Lett. **5**, 1245 (1986).
[30] N. N. Nemeth, O. Jadaan, J. P. Palko, J. Mitchell, and C. A. Zorman, Proceedings of the MEMS: Mechanical and Measurement Symposium 2001, p. 46.
[31] A. J. Hallinan, Jr., J. Quality Technol. **25**, 2 (1993).